Mobility of the two-dimensional electron gas at selectively doped n-type $Al_xGa_{1-x}As/GaAs$ heterojunctions with controlled electron concentrations

Kazuhiko Hirakawa and Hiroyuki Sakaki
Institute of Industrial Science, The University of Tokyo, 7-22-1 Roppongi, Minato-ku, Tokyo 106, Japan
(Received 16 December 1985)

We describe our systematic study of the two-dimensional electron mobilities μ of n-type $Al_xGa_{1-x}As/GaAs$ heterojunctions, in particular their dependence on the electron concentration N_s and the temperatures T, in a variety of field-effect transistors in which the impurity locations are precisely controlled to vary μ over the wide range of 5×10^3 to 1.5×10^6 cm^2/V s. It is found that μ increases with increasing N_s in the temperature range of 10 to 300 K. The measured mobilities are compared with theoretical calculations. The observed dependence of μ on N_s at low temperatures is shown to be in excellent agreement with the theory of ionized-impurity scattering, whereas the high-temperature data disagree with the existing theory of polar-optical phonon scattering. A quantitative study has been successfully made on the effect of an undoped $Al_xGa_{1-x}As$ spacer layer, which enhances not only μ itself but also the slope in $\log\mu$-$\log N_s$ characteristics. The presence of both positive and negative temperature dependences of μ at low temperatures ($T<40$ K) is noted, and its connection with the effects of nondegeneracy and lattice scattering is also discussed.

I. INTRODUCTION

The two-dimensional electron gas (2D EG) accumulating on the GaAs side of a selectively-doped n-type $Al_xGa_{1-x}As/GaAs$ heterojunction is known to exhibit very high mobility because of the spatial separation of electrons from donor impurities in the $Al_xGa_{1-x}As$ (Refs. 1 and 2). Although a large number of investigations have been done on the high-mobility nature of this system, experiments have been concentrated mostly on the temperature dependence of mobilities in samples with fixed electron concentrations[3,4] and, hence, provided only limited understanding of the relative importance of various scattering mechanisms. It has been suggested that the mobilities at high and intermediate temperatures are mainly dominated by the lattice scatterings due to polar-optical phonons and acoustic phonons, whereas the low-temperature mobilities are primarily determined by the scattering by ionized impurities. Since all of these scattering mechanisms depend not only on the temperature, but also on the kinetic energy and the quantized wave function of electrons,[5–16] the relative importance of the scattering mechanisms can be clarified only by making a systematic measurement of mobilities as a function of these parameters and by detailed comparison with theoretical models.[17–19]

In this work, we measured the electron mobilities μ in a variety of heterojunction samples as a function of the electron concentration N_s as well as the temperature T, and compared them with theoretical calculations. The electron concentration N_s was varied by gating electric fields in a field-effect transistor (FET) configuration not only to study all the possible situations encountered in FET operations, but also to eliminate the possible experimental ambiguities that might be present in former experimental works, where N_s was varied by persistent photoconductivity (PPC).[1,2,20,21] Note that the PPC effect may affect the concentration of ionized impurities and/or the band profiles. It will be shown in this work that μ increases with increasing N_s in the entire temperature range studied here (10—300 K), as long as the effect of parallel conduction of low-mobility electrons in the $Al_xGa_{1-x}As$ is made negligibly small. Furthermore, we study the N_s dependence of the low-temperature electron mobility and its dependence on the thickness W_{sp} of the undoped $Al_xGa_{1-x}As$ "spacer" layer. It will be shown that the larger W_{sp} leads not only to an enhancement in the mobility but also to a steeper slope in the μ-N_s characteristics, in excellent agreement with theoretical predictions.[6] It is also found that in low-mobility samples ionized-impurity scattering plays a significant role, especially in the low-N_s region, and gives rise to a strong positive temperature dependence for μ.

II. SCATTERING THEORY OF TWO-DIMENSIONAL ELECTRONS IN $Al_xGa_{1-x}As/GaAs$ HETEROJUNCTIONS

The scattering theories of the two-dimensional (2D) carriers in the $Al_xGa_{1-x}As/GaAs$ heterojunction system have been developed by several authors.[5–16] The calculated mobilities, however, differ from each other, depending on the theoretical models adopted in their calculations. Therefore, we summarize briefly the theoretical models adopted in our calculations.

The electronic state in the channel is characterized by subband index n and a 2D wave vector $\mathbf{k}=(k_x,k_y)$ along the heterointerface. Its wave function and energy are, respectively, given by

$$\Psi_{n,\mathbf{k}}(\mathbf{r},z)=f_n(z)\exp(i\mathbf{k}\cdot\mathbf{r}) , \quad (1)$$

$$E_n(\mathbf{k})=E_n+\hbar^2k^2/2m^* , \quad (2)$$

where $f_n(z)$ denotes the quantized wave function, m^* the

electron effective mass in GaAs, and $\hbar$ the reduced Planck constant.

In the scattering process of 2D carriers, the momentum conservation in the z direction in the three-dimensional (3D) case is replaced by the integral[7]

$$M_{\rm II}^2 = \int M_{\rm III}^2 \, |I(q_z)|^2 dq_z \ . \tag{3}$$

Here, $M_{\rm II}$ and $M_{\rm III}$ are the bare scattering matrix elements in two dimensions and three dimensions, respectively, and q_z is the wave vector normal to the heterointerface. $I(q_z)$ is defined by[7]

$$I(q_z) \equiv I_{mn}(q_z) \equiv \int f_m f_n \exp(iq_z z) dz \ . \tag{4}$$

In the following, we assume that electrons populate only the lowest subband, neglecting the contribution of intersubband scattering. Unless otherwise specified, we adopt for $f(z)$ the Fang-Howard variational wave function,[22]

$$f(z) = (\tfrac{1}{2} b^3 z^2)^{1/2} \exp(-\tfrac{1}{2} bz) \tag{5}$$

with variational parameter b, which is given by

$$b = (12 m^* e^2 / \kappa_0 \epsilon_0 \hbar^2)^{1/3} (N_{\rm depl} + \tfrac{11}{32} N_s)^{1/3} \ , \tag{6}$$

where e is the elemental charge, ϵ_0 the dielectric permittivity, κ_0 the static dielectric constant of GaAs, $N_{\rm depl}$ the areal concentration of depletion charges in the GaAs, and N_s the concentration of 2D electron gas. Substitution of (5) into (4) yields

$$|I(q_z)|^2 = \frac{b^6}{(b^2+q_z^2)^3} \ . \tag{7}$$

Since the scattering matrix element $M_{\rm III}$ in three dimensions is well established,[23] we can calculate $M_{\rm II}$ and the differential scattering cross sections $\nu(\theta)$ for various scattering mechanisms. We consider here the ionized-impurity scattering, the acoustic-phonon scattering, and the polar-optical phonon scattering.

In elastic scattering processes the screening effect is taken into account by dividing $M_{\rm II}$ by $S(q)$ (Ref. 24)

$$S(q) = 1 + e^2 F(q) \Pi(q) / 2\kappa_0 \epsilon_0 q \ , \tag{8}$$

where $F(q)$ is the form factor defined by

$$F(q) \equiv \int_0^\infty dz \int_0^\infty dz' [f(z)]^2 [f(z')]^2 \times \exp(-q\,|z-z'|) \ . \tag{9}$$

Here, $\mathbf{q} = \mathbf{k}_2 - \mathbf{k}_1$ is the 2D scattering wave vector from the initial state $\mathbf{k}_1$ to the final state $\mathbf{k}_2$, and $q = |\mathbf{q}|$. If we put the variational wave function (5) into (9), we have[16]

$$F(q) = b(8b^2 + 9bq + 3q^2)/8(b+q)^3 \ . \tag{10}$$

$\Pi(q)$ is the static polarizability function, which depends on both T and q. Following Maldague,[25] we calculate $\Pi(q)$:

$$\Pi(q,T,\xi) = \int_0^\infty \frac{\Pi(q,0,\xi')}{4k_B T \cosh^2[(\xi-\xi')/2k_B T]} d\xi' \ , \tag{11}$$

where ξ is the Fermi energy, k_B the Boltzmann constant, and $\Pi(q,0,\xi)$ is the polarizability function at $T=0$, which is given by

$$\Pi(q,0,\xi) = \frac{m^*}{\pi\hbar^2} \left\{ 1 - u(q-2k_F) \left[1 - \left[\frac{2k_F}{q} \right]^2 \right]^{1/2} \right\} , \tag{12}$$

where $u(x)$ is the usual unit step function and k_F the Fermi wave vector.

Differential scattering cross section $\nu_I(\theta)$ due to the ionized impurities with the charge Ze is given by[5,6]

$$\nu_I(\theta) = \frac{m^* Z^2 e^4}{8\pi\hbar^3 \kappa_0^2 \epsilon_0^2} \int dz_i \left[\frac{F(q,z_i)}{qS(q)} \right]^2 N(z_i)(1-\cos\theta) \ , \tag{13}$$

where $N(z_i)$ is the impurity distribution, θ the scattering angle between $\mathbf{k}_1$ and $\mathbf{k}_2$, and, then, $q = 2k\,|\sin(\theta/2)|$ with $k = |\mathbf{k}_1| = |\mathbf{k}_2|$. The form factor $F(q,z_i)$ is defined by[5,6]

$$F(q,z_i) \equiv \int dz \, |f(z)|^2 \exp(-q\,|z_i - z|) \ . \tag{14}$$

Scattering by acoustic phonons has two coupling modes; namely, deformation potential coupling and piezoelectric coupling. Since both scattering processes are virtually elastic, the screening effect is expected to be efficient. When all the acoustic modes are fully excited, the differential scattering cross section due to deformation potential scattering $\nu_{\rm DP}(\theta)$ is given by[7,8]

$$\nu_{\rm DP}(\theta) = \frac{3b D^2 m^* k_B T (1-\cos\theta)}{32\pi\hbar^3 c_L S(q)^2} \ , \tag{15}$$

where D is the deformation potential constant, and c_L the longitudinal elastic constant. For scattering through piezoelectric coupling, we adopt the results of Price,[7,9]

$$\nu_{PE}(\theta) = \frac{(eh_{14})^2 m^* k_B T}{4\pi\hbar^3} \times \frac{1}{qS(q)^2} \left[\frac{9}{32c_L} f_L(w) + \frac{13}{32c_T} f_T(w) \right] \times (1-\cos\theta) \ , \tag{16}$$

where h_{14} is the relevant piezoelectric tensor component and c_T the transverse elastic constant. $f_L(w)$ and $f_T(w)$ are the dimensionless form factor for longitudinal and transverse phonon modes, respectively, and are given by

$$f_L(w) = (1+6w+12w^2+2w^3)/(1+w)^6 \ , \tag{17}$$

$$f_T(w) = (13+78w+72w^2+82w^3 + 36w^4+6w^5)/13(1+w)^6 \ , \tag{18}$$

with

$$w = q/b \ . \tag{19}$$

Since scattering by polar-optical phonons is an inelastic process, only an approximate form for the scattering rate can be obtained in a closed form. In the relaxation-time approximation, which neglects the "in-scattering" term in

TABLE I. Values of GaAs material constants used in the calculation.

Electron effective mass	$m^*=0.067\ m_0$
Static dielectric constant	$\kappa_0=12.91$
Optical dielectric constant	$\kappa_\infty=10.92$
Deformation potential constant	$D=13.5$ eV
LO-phonon energy	$\hbar\omega_{LO}=36.5$ meV
Piezoelectric constant	$h_{14}=1.2\times10^9$ V/m
Longitudinal elastic constant	$c_L=1.44\times10^{11}$ N/m^2
Transverse elastic constant	$c_T=0.49\times10^{11}$ N/m^2
Band-gap energy	$E_g=1.52$ eV

the scattering process, we have

$$\nu_{PO}\theta=\frac{m^*e^2\hbar\omega_{LO}}{8\pi^2\hbar^3\epsilon_0}\left[\frac{1}{\kappa_\infty}-\frac{1}{\kappa_0}\right]\frac{1}{1-f_0(E)}\times\left[[1-f_0(E+\hbar\omega_{LO})]N_q\int\frac{|I(q_z)|^2}{q_+^2+q_z^2}dq_z+[1-f_0(E-\hbar\omega_{LO})]u(E-\hbar\omega_{LO})(N_q+1)\times\int\frac{|I(q_z)|^2}{q_-^2+q_z^2}dq_z\right], \quad (20)$$

where $\hbar\omega_{LO}$ denotes the longitudinal-optical (LO) phonon energy, κ_∞ the optical dielectric constant, N_q the phonon occupation number, $f_0(E)$ the Fermi-Dirac distribution function, q_+ and q_- the 2D scattering wave vectors in the phonon absorption and emission process, respectively. N_q and $f_0(E)$ are, respectively, given by

$$N_q=\frac{1}{\exp(\hbar\omega_{LO}/k_BT)-1}, \quad (21)$$

$$f_0(E)=\frac{1}{\exp[(E-E_F)/k_BT]+1}. \quad (22)$$

In the calculation we neglect the screening effect, because the LO phonon frequency is high.

The inverse of the momentum relaxation time is given by

$$\frac{1}{\tau(E)}=\int_0^{2\pi}\nu(\theta)d\theta \quad (23)$$

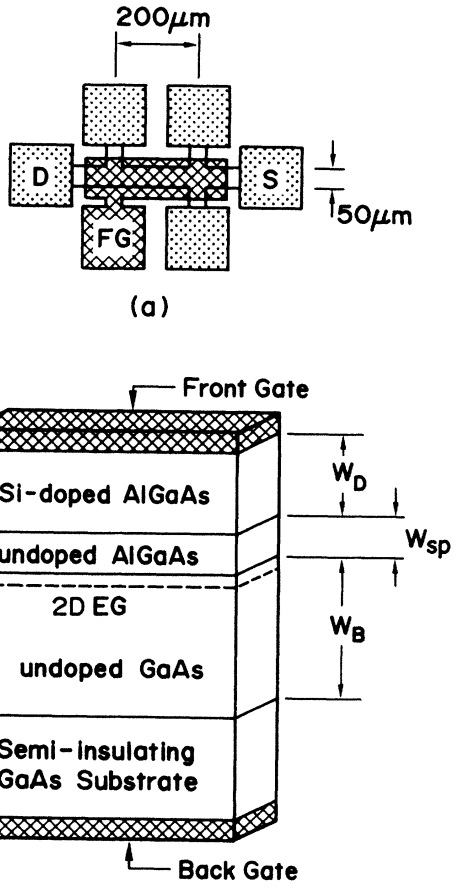

FIG. 1. (a) The geometrical pattern of the Hall-bridge device. (b) Cross-sectional view of the selectively doped n-type $Al_xGa_{1-x}As/GaAs$ single heterostructure sample with gate electrodes.

with

$$\nu(\theta)=\nu_I(\theta)+\nu_{DP}(\theta)+\nu_{PE}(\theta)+\nu_{PO}(\theta). \quad (24)$$

The mobility is, then, given by

$$\mu=\frac{e}{m^*}\langle\tau\rangle \quad (25)$$

TABLE II. Structural parameters of the samples. W_B is the thickness of the undoped GaAs buffer layer, W_{sp} is the thickness of the undoped $Al_xGa_{1-x}As$ spacer, W_D is the thickness of the Si-doped $Al_xGa_{1-x}As$ layer, N_D is the Si-doping level in the $Al_xGa_{1-x}As$ layer, x is the AlAs mole fraction in the $Al_xGa_{1-x}As$ alloy layer, FG is the front-gate electrode, and BG is the back-gate electrode.

Sample	W_B (m)	W_{sp} (nm)	W_D (nm)	N_D (10^{18} cm^{-3})	x	Gate
1A (R-98 FET-D)	1.1	0	84.0	0.66	0.3	FG
1B (R-98-5TA)	1.1	0	100	0.66	0.3	
2A (R-73 FET-A)	1.1	4.5	117.0	0.54	0.3	FG
2B (R-73 FET-B)	1.1	4.5	122.6	0.47	0.3	FG,BG
3 (R-76 FET-B)	1.1	18.0	95.0	0.43	0.3	FG
4 (R-248-5TA)	1.0	5.0	100	0.34	0.3	
5 (R-249-5TA)	1.0	10.0	100	0.34	0.3	
6 (R-250-5TA)	1.0	20.0	100	0.34	0.3	
7 (R-251-5TA)	1.0	30.0	100	0.34	0.3	

with

$$\langle \tau \rangle = \frac{\int_0^\infty \tau(E) E \frac{\partial f_0(E)}{\partial E} dE}{\int_0^\infty E \frac{\partial f_0(E)}{\partial E} dE} . \quad (26)$$

Material parameters used in the calculation below are listed in Table I.

III. EXPERIMENTAL METHOD AND DEPENDENCES OF MOBILITY ON ELECTRON CONCENTRATIONS

All the samples used in this study were grown on Cr-doped semi-insulating (100) GaAs substrates by molecular beam epitaxy (MBE). n-type $Al_xGa_{1-x}As$/GaAs single heterojunctions were prepared by growing successively a 1-μm thick undoped GaAs buffer layer, an undoped $Al_xGa_{1-x}As$ spacer layer with thickness $W_{sp}(=0-30.0$ nm), a 80—120 nm-thick Si-doped $Al_xGa_{1-x}As$ layer with the donor concentration $N_D(=3-7\times10^{17}$ cm$^{-3})$, and a 10-nm-thick undoped GaAs cap layer. The AlAs mole fraction in the $Al_xGa_{1-x}As$ is 0.3, and the growth rate is typically 0.45 μm/h for GaAs. Using some of these wafers, we fabricated depletion-mode FET's with Hall-bar geometry (Fig. 1). First, AuGe was evaporated and patterned using the lift-off technique to form the source/drain and potential-probe electrodes. Alloying was done at about 400°C for 1 min in Ar ambient to form good ohmic contacts. The Hall-bar geometry was photolithographically defined and mesa-etched in $1H_3PO_4$:$1H_2O_2$:$8H_2O$ solution for 2 min 30 sec at room temperature. The channel is 50-μm wide and 600-μm long and the potential-probe spacing is 200 μm. Then, the $Al_xGa_{1-x}As$ layer was thinned by etching to remove the electrically neutral region in the $Al_xGa_{1-x}As$. The gate electrode was formed by depositing Al, which was patterned by the lift-off method. Table II summarizes the structural parameters of the samples studied here. Hall measurements were performed under low magnetic field by supplying a constant current (typically ~1 μA) in a closed cycle refrigerator system. The mobility μ and the electron concentration N_s were determined as functions of gate voltages.

To confirm FET actions, the electron concentration N_s was measured by the Hall effect as functions of gate voltage (V_{gs}). Figure 2 shows two typical data. Figure 2(a) is the result for the sample 1A, in which the effect of parallel conduction of the low-mobility electrons in the $Al_xGa_{1-x}As$ is negligibly small, and Fig. 2(b) is, on the other hand, for the sample 3, in which the effect of parallel conduction cannot be neglected. In all the samples studied here, no shifts of the threshold voltages V_{th} were observed in the temperature range from 8.9 to 125 K. This indicates that the electron occupation of the donors in the $Al_xGa_{1-x}As$ is not affected by the temperature in this temperature range. Hence, the $Al_xGa_{1-x}As$ layer works as a simple insulator, resulting in the quasilinear increase of N_s with V_{gs}. The saturation of N_s against V_{gs}, which is observed for large positive V_{gs}, is due to the formation of an electrically neutral region in the $Al_xGa_{1-x}As$ layers, as quantitatively discussed elsewhere.[26–28] The saturation value N_{ssat} decreases drastically as W_{sp} increases, in accordance with the theoretical prediction.[26]

When T is raised above 135 K, however, the threshold voltage V_{th} starts to shift towards the negative direction.

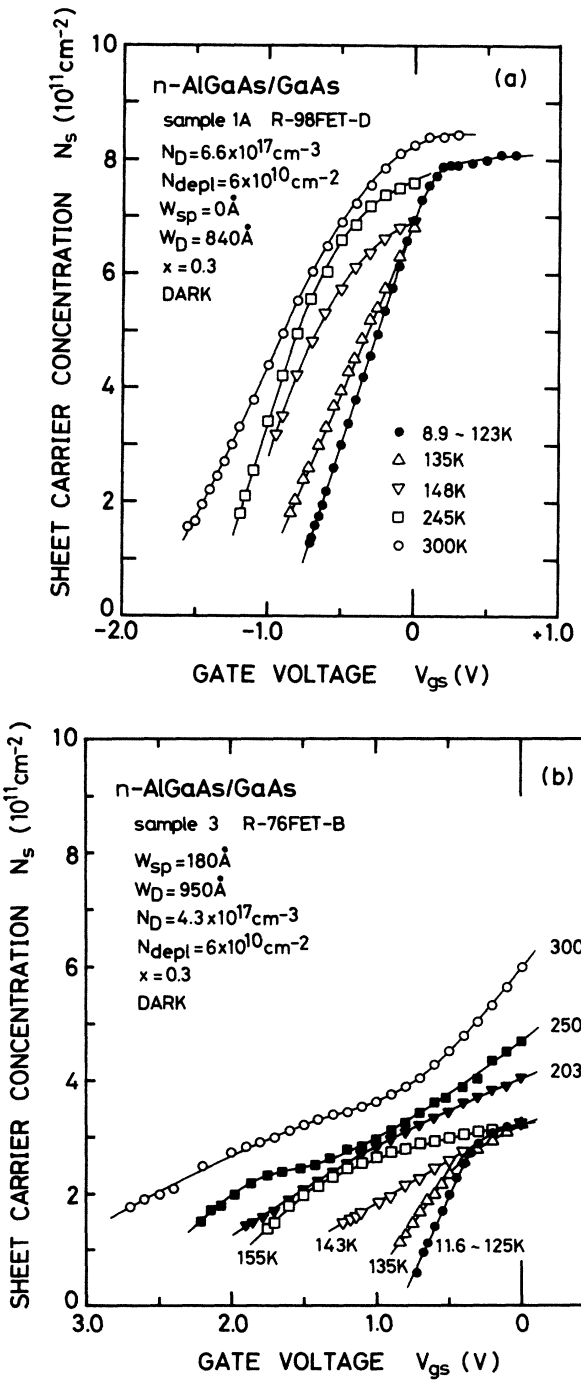

FIG. 2. Sheet electron concentration N_s is plotted as a function of gate-source voltage V_{gs}, with temperature T as a parameter. (a) Sample 1A with $W_{sp}=0$; (b) sample 3 with $W_{sp}=18.0$ nm.

Simultaneously, N_s-V_{gs} curves become less steep, leading to a reduction of the effective gate capacitance. These phenomena are more pronounced in the sample 3 [Fig. 2(b)], which has a thicker Si-doped $Al_xGa_{1-x}As$ layer, suggesting that these phenomena are related with the thermal activation of the electrons trapped by the deep donors in the $Al_xGa_{1-x}As$ (Refs. 29 and 30). A large increase of N_s in the sample 3 at around $V_{gs} \sim 0$ and $T > 203$ K is due to the parallel conduction of the low-mobility electrons in the $Al_xGa_{1-x}As$.

Using these FET samples, we measured the electron mobility μ as functions of electron concentration N_s with temperature T as a parameter. Figures 3(a)–3(c) show the results of such measurements for three samples with different thicknesses of the spacer W_{sp} (=0, 4.5, and 18.0 nm). It is noted that μ increases with increasing N_s in the entire temperature range studied here (10–300 K), except the high-temperature data of the sample 3. In sample 3 the reduction of μ is observed with increasing N_s at $T > 203$ K, which is caused by the parallel conduction of

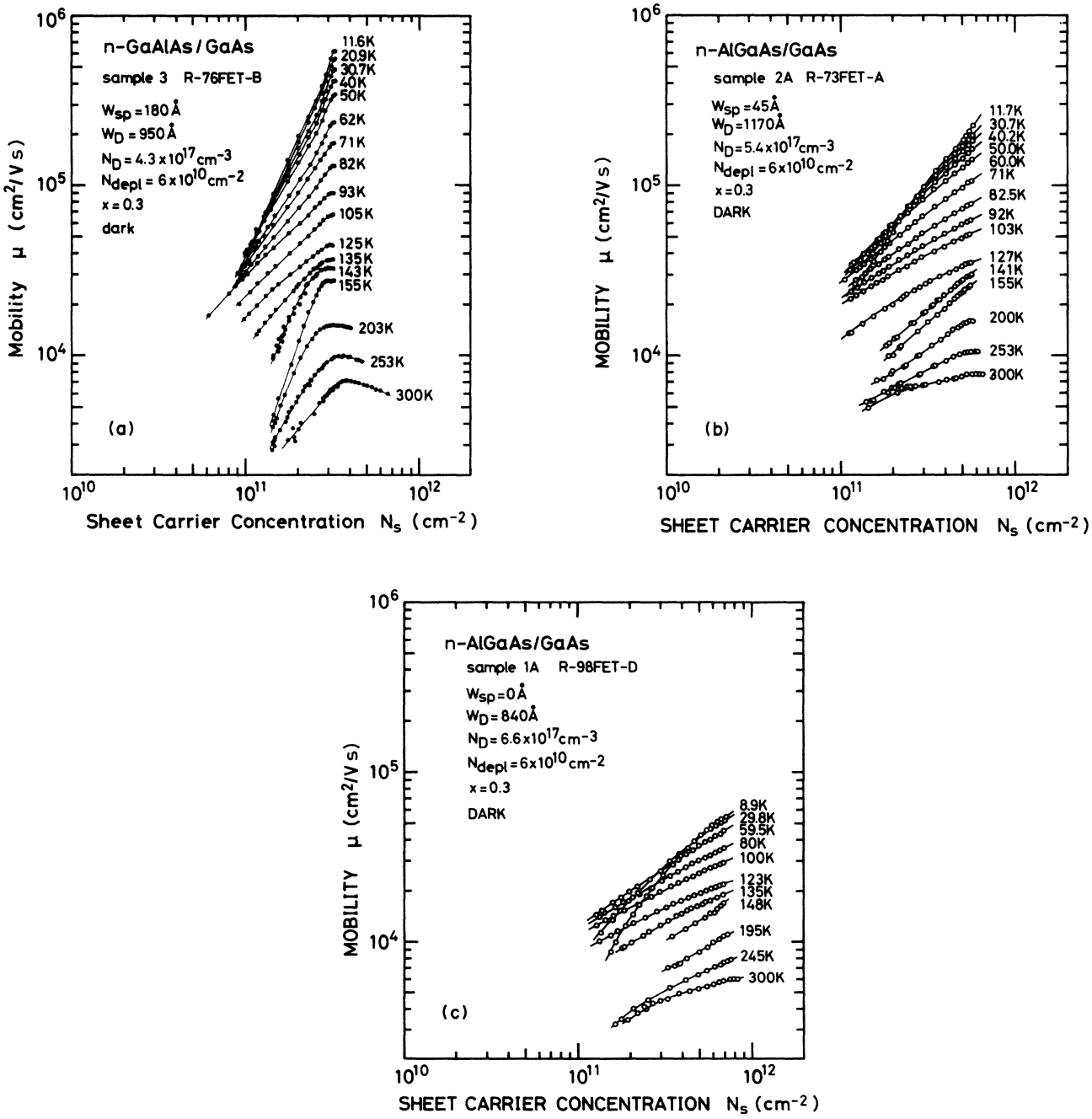

FIG. 3. Electron mobility μ is plotted as a function of electron concentration N_s, with temperature T as a parameter. N_s is varied by the gate-electric field in a field-effect transistor configuration. (a) $W_{sp} = 18.0$ nm (sample 3), (b) $W_{sp} = 4.5$ nm (sample 2A), and (c) $W_{sp} = 0$ nm (sample 1A).

the low-mobility electrons in the $Al_xGa_{1-x}As$. It should be noted that μ increases with increasing N_s even at 300 K, where electrons are mainly scattered by polar-optical phonons. This fact is in contrast with the Si-MOS inversion layer case, in which μ varies as $\mu \propto N_s^{-1/3}$ at around 300 K (Refs. 31 and 32), where electrons are mainly scattered by acoustic phonons through deformation potential coupling.

We examine below more closely the μ-N_s characteristics in each temperature range.

A. Low-temperature range ($T \sim 10$ K)

In the low-temperature range, μ is strongly dependent on N_s and varies as $\mu \propto N_s^{1.1}$ for $W_{sp}=0$ nm (sample 1A), $\mu \propto N_s^{1.3}$ for $W_{sp}=4.5$ nm (sample 2A), and $\mu \propto N_s^{1.7}$ for $W_{sp}=18.0$ nm (sample 3), respectively. Such strong positive N_s dependences suggest that the dominant scatterers are characterized by the potential $V(r)$ whose Fourier component $V(q)$ diminishes strongly when q is raised. Hence, the scatterers are most likely the ionized-impurity ions in the $Al_xGa_{1-x}As$. This can be confirmed by comparison with theoretical calculations. Figure 4(a) shows the N_s-dependence of μ at 11.7 K in sample 2A. The results of numerical calculations are also plotted in the figure. Note that electrons are predominantly scattered by ionized impurities in the $Al_xGa_{1-x}As$ and that scattering by acoustic phonons has its effect only when $\mu > 10^6$ cm^2/V s. Detailed discussions of the μ-N_s characteristics at low temperatures and, in particular, of their dependences on W_{sp} will be made in Sec. IV.

B. Intermediate-temperature range (10 K $< T <$ 40 K)

In this temperature range, μ is described as $\mu \propto N_s^{\gamma}$, the exponent γ being a function of temperature. As shown in Figs. 3, γ decreases with increasing T, from 1.1 to 0.5 for $W_{sp}=0$ nm, from 1.4 to 0.5 for $W_{sp}=4.5$ nm, and from 1.7 to 1 for $W_{sp}=18.0$ nm. This tendency reflects the increasing contribution of acoustic-phonon scattering with the rise in T, since the acoustic-phonon scattering is less dependent on N_s ($\mu_{DP} \propto N_s^{-1/3}$ for deformation potential coupling, $\mu_{PE} \propto N_s^{1/2}$ for piezoelectric coupling) than the ionized-impurity scattering ($\mu_I \propto N_s^{1 \sim 1.5}$).

This situation is shown in Fig. 4(b), where N_s dependence of μ at 40.2 K in sample 2A is plotted together with the result of numerical calculations. In the acoustic-phonon scattering process, the deformation potential coupling dominates over the piezoelectric coupling. Although the slope of measured μ-N_s characteristics is a little steeper than that of calculated ones, the agreement between experiments and theories is rather good. The polar-optical phonon scattering has negligible contribution to μ at this temperature.

C. High-temperature range (40 K $< T <$ 300 K)

In the high-temperature range, where scattering due to the polar-optical phonon increases its strength exponentially with the rise in T, μ still increases with N_s as $\mu \propto N_s^{\gamma}$ with the exponent γ being 0.3–2.

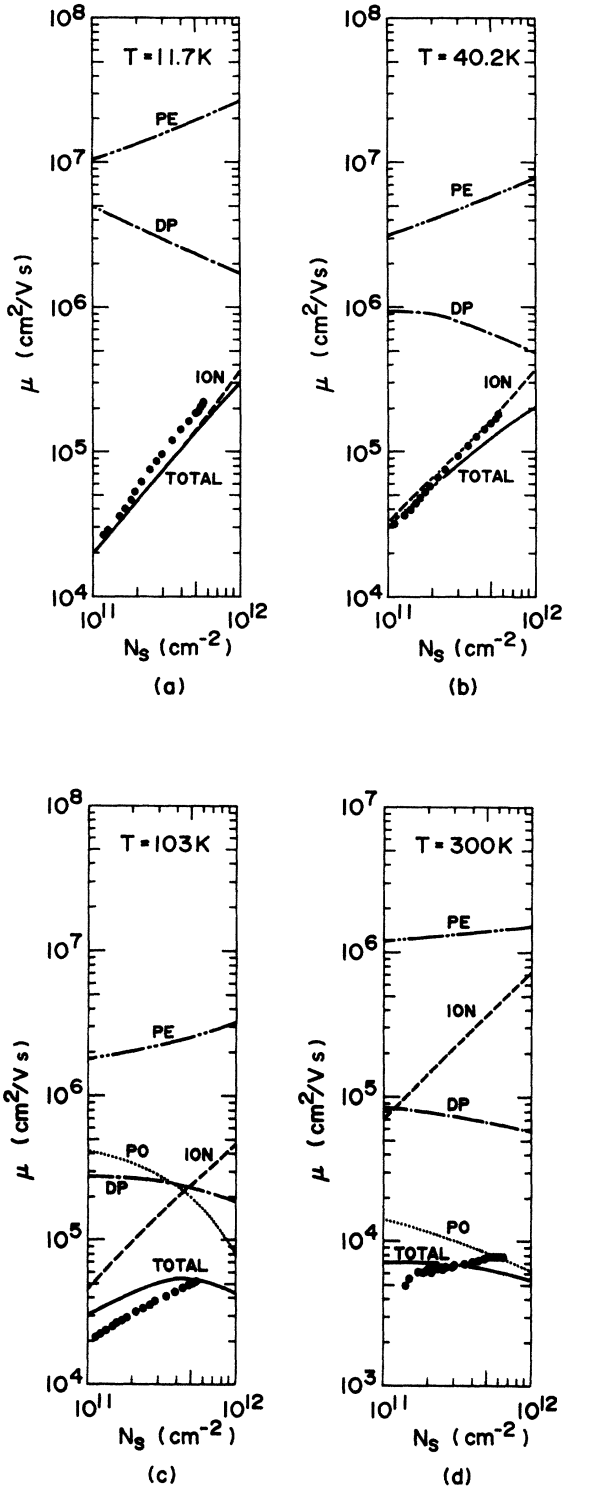

FIG. 4. Electron mobility in sample 2A versus electron concentration N_s at different temperatures; (a) 11.7 K, (b) 40.2 K, (c) 103 K, and (d) 300 K. Measured mobilities are plotted by full circles. Calculated mobilities limited by individual scattering mechanisms are also plotted in the figure; ionized-impurity scattering (ION), acoustic-phonon scattering via deformation-potential coupling (DP), acoustic-phonon scattering via piezoelectric coupling (PE), and polar-optical phonon scattering (PO). The total mobility (TOTAL) is plotted by solid lines.

Figure 4(c) shows the μ-N_s characteristics at 103 K in sample 2A. Although theoretical calculation predicts that phonon scattering dominates μ in the high-N_s range and gives rise to a negative N_s dependence in μ, measured mobility increases monotonically with N_s and somewhat lower than that predicted. The origin of such a discrepancy is not clear at present.

Figure 4(d) shows the μ-N_s characteristics at 300 K in sample 2A together with the results of the theoretical calculations. It is noteworthy that measured μ increases with N_s even near the room temperature, where electrons are predominantly scattered by polar-optical phonons. This is in contrast with the two-dimensional electron mobility in Si-MOS inversion layers, where μ decreases with N_s as $\mu \propto N_s^{-1/3}$ due to the enhancement of electron-phonon coupling.[31,32] This positive N_s dependence of μ cannot be understood by the existing theory of polar-optical phonon scattering;[13,15] the experiments shown in Figs. 4(c) and 4(d) suggest that the mobility limited by polar-optical phonon scattering should increase with N_s or, at least, be almost independent of N_s, calling for the further refinement of the theoretical study. Also note in the figure that the calculated mobilities are somewhat lower than the measured ones. This is due to neglecting the in-scattering term in the calculation of the polar-optical phonon scattering process.

In Figs. 3(a)—3(c), a remarkable increase of the exponent γ is clearly seen in the temperature range of around 150 K and higher. This temperature range coincides with the range where the threshold voltage V_{th} starts to shift towards the negative direction. This fact suggests that the increase of γ is possibly ascribed to the increasing rate of ionized-impurity scattering through the gate-voltage induced thermal ionization of the deep donors in the $Al_xGa_{1-x}As$ at around 150 K.

IV. SYSTEMATIC COMPARISON OF LOW-TEMPERATURE MOBILITIES WITH THE THEORY OF THE IONIZED-IMPURITY SCATTERING

It is often suggested that the low-temperature mobility of electrons in n-type $Al_xGa_{1-x}As/GaAs$ heterojunctions is dominated by the ionized-impurity scattering. Indeed, the suppression of the ionized-impurity scattering by use of a spacer layer leads to a dramatic and systematic improvement of μ at low temperatures, reaching 1.5×10^6 cm^2/V s at 1.0 K when $W_{sp}=30$ nm (Fig. 5). In spite of the importance of the ionized-impurity scattering, only a few works have been done on detailed comparison of experimental data with theoretical predictions.[6] In this section, we make a systematic comparison between experiments and theories and discuss, in particular, the N_s dependence of μ for three FET samples with different spacer thicknesses.

First, we measured the mobilities at 1 K for four samples with different spacer thicknesses ($W_{sp}=5.0$, 10.0, 20.0, and 30.0 nm), which were grown in rapid succession within 20 hours to minimize possible fluctuations of the growth conditions. The doped $Al_xGa_{1-x}As$ layers are 100-nm thick and thick enough not to be completely depleted. The donor concentration N_D in the $Al_xGa_{1-x}As$ is calibrated to be 3.4×10^{17} cm^{-3} by Hall measurements on the bulk GaAs sample, which was grown in the same run. In Fig. 6, measured mobilities are plotted as a function of W_{sp}. It is noted that μ increases monotonically with increasing W_{sp} in the range of W_{sp} studied here. Calculated mobilities are also plotted in the figure by solid lines for different residual-impurity concentrations N_{res}. Here, we assume that the residual impurities are acceptors and uniformly distributed both in the GaAs buffer layer and in the $Al_xGa_{1-x}As$ spacer layer ($N_{res}=N_B=N_{sp}$). In the calculation, the electron wave function was approximated by Eq. (5) (Ref. 22). We assume that the effect of interface charges is negligibly small. Note in the figure that as the residual impurities increase, μ decreases monotonically and tends to show its peak, when plotted as a function of W_{sp}. The good agreement between measured data and theoretical results in Fig. 6 indicates that the residual impurity level in our heterojunctions is as low as 1×10^{14} cm^{-3}, and that electrons are predominantly scattered by the ionized donor impurities in the $Al_xGa_{1-x}As$ at low temperatures. Concurrently, the measured electron concentrations N_s (shown by triangles in Fig. 6) are in excellent agreement with the calculated results (dashed line in Fig. 6), supporting the validity of our theoretical model.

Next, we discuss mobilities at 12 K as functions of N_s. Since the low-temperature mobility in high purity n-type $Al_xGa_{1-x}As/GaAs$ heterojunctions is dominated by the scattering due to the intentionally doped donor impurities in the $Al_xGa_{1-x}As$ and is inversely proportional to the donor concentration N_D (as long as N_s is kept constant),

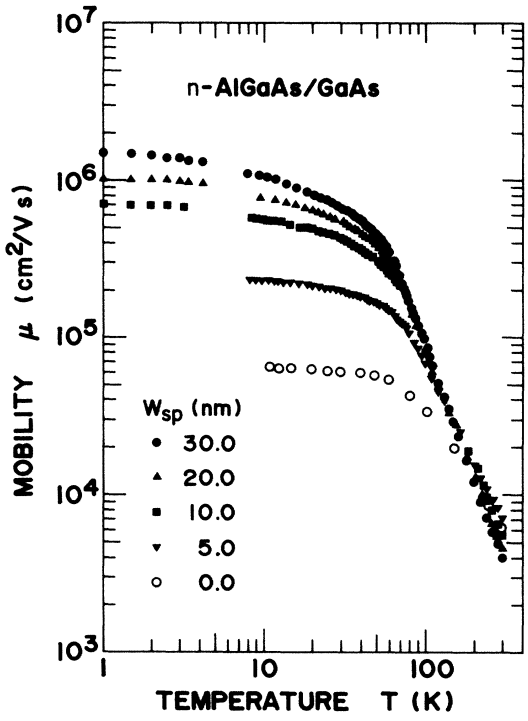

FIG. 5. Temperature dependence of electron mobility μ. Thickness of spacer layer W_{sp} is a parameter.

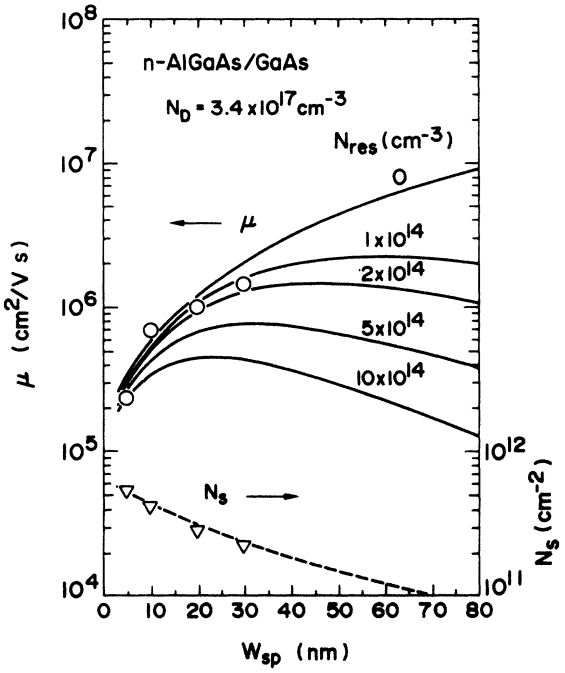

FIG. 6. Dependences of low-temperature (1 K) mobilities and electron concentrations on spacer thicknesses W_{sp}. Calculated mobilities are plotted by solid lines, with residual impurity level N_{res} as a parameter. Calculated electron concentrations are also shown by a dashed line when $N_{res}=1\times10^{14}$ cm^{-3}.

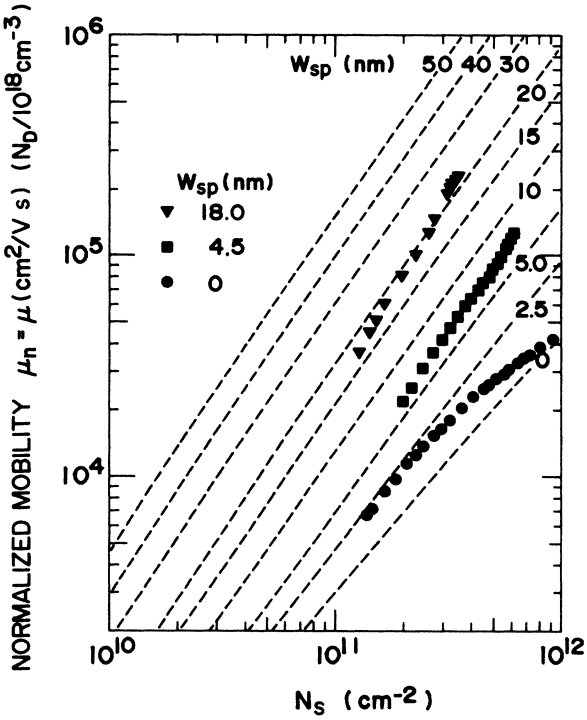

FIG. 7. Normalized mobilities μ_n $(=\mu N_D)$ are plotted as functions of N_s, with spacer thickness W_{sp} as a parameter; triangles for $W_{sp}=18.0$ nm (sample 3), squares for $W_{sp}=4.5$ nm (sample 2A), and circles for $W_{sp}=0$ (sample 1A). Calculated normalized mobilities are also plotted in the figure by dashed lines.

we define for the sake of convenience the normalized mobilities by $\mu_n \equiv \mu \times N_D$. In Fig. 7, we plot μ_n by circles, squares, and triangles for the three samples with $W_{sp}=0$, 4.5, and 18.0 nm, respectively. Three features are to be noted: (1) μ_n increases monotonically with N_s as mentioned in Sec. III; (2) μ_n is greater for samples with thicker spacer layers; and (3) the slopes in $\log\mu_n$-N_s characteristics become steeper, when W_{sp} is increased. All of these features can be qualitatively understood by considering the following natures of the Coulomb potential. When an ionized impurity is located (in the $Al_xGa_{1-x}As$) at some distance z_i away from the heterointerface, then the bare Coulomb potential is proportional to $1/R=1/(x^2+y^2+z_i^2)^{1/2}$. The 2D Fourier decomposition of this term can be expressed as

$$1/R=\int d^2\mathbf{q}\exp(i\mathbf{q}\cdot\mathbf{r})\exp(-q\,|\,z_i\,|\,)/2\pi q\ . \tag{27}$$

Here, $\mathbf{r}=(x,y)$ is the 2D coordinate vector along the heterointerface, $\mathbf{q}$ is the 2D wave vector, and $q=|\,\mathbf{q}\,|$. Equation (27) indicates that the high-frequency component of the Coulomb potential decreases very rapidly with q. This implies that when the Fermi momentum is increased by raising N_s, then the effective scattering potential becomes weak, resulting in the increase in mobility, in accordance with the observations. Equation (27) also indicates that the use of a spacer layer of thickness W_{sp} increases z_i and, thereby, reduces the Coulomb potential by a factor of $\exp(-qW_{sp})$, resulting directly in the increase of μ. This explains the monotonic increase of μ with W_{sp}. The same factor $\exp(-qW_{sp})$ explains also the observed increase of slopes in μ_n-N_s characteristics, since the reduction of the potential by the spacer layer is particularly effective for the high-q component, which dominates the mobility at high electron concentration.

In order to make quantitative comparison in details, the theoretical calculations of mobility limited by the ionized-impurity scattering were performed. In this calculation the electron wave function $f(z)$ is approximated by the modified variational wave function which takes into account the penetration of the wave function into the $Al_xGa_{1-x}As$ layer.[6] In the calculation, we need to know the following quantities: the thicknesses W_D, W_{sp}, and W_B, and the impurity concentrations N_D, N_{sp}, and N_B of three constituent layers, where the subscripts D, sp, and B stand, respectively, for the Si-doped $Al_xGa_{1-x}As$ layer, the undoped $Al_xGa_{1-x}As$ spacer layer, and the undoped GaAs buffer layer. We determined N_D from the maximum value of N_s which can be induced by the gate electric field.[26] We assume here that the spacer and the buffer layer are nearly free from ionized impurities, and set $N_{sp}=N_B=0$. Note that the contribution of residual impurities to μ is negligibly small when $N_B=N_{sp}=1\times10^{14}$ cm^{-3}, as long as W_{sp} is in the range studied here (0—18 nm). The heterointerface was assumed to be free from interface charges. The depth-integrated concentration N_{depl} of the depletion layer charges in the GaAs was evaluated to be 0.6×10^{11} cm^{-2}, by assuming that

N_{depl} is determined not only by the residual impurity N_B in the GaAs but by the Fermi level at the interface between the epilayer and the semi-insulating substrate, which is clamped at the middle of the GaAs bandgap, as noted by us previously.[33] The total $Al_xGa_{1-x}As$ thickness ($W_D + W_{sp}$) was determined by measuring the low-temperature gate capacitance, and W_{sp} was determined from the growth rates. Since the value of W_D thus determined is in the range from 84 to 120 nm, we set W_D used in the calculation to be 100 nm for simplicity. This can be justified, because μ is primarily dominated by the scattering due to impurities which are located within the distance of 50 nm from the spacer and, hence, does not depend on W_D sensitively. W_B was determined from the growth rates.

The mobility thus calculated is plotted by the dashed lines in Fig. 7. Note that the overall agreement between the theory and the experiment is very good, although no fitting parameters are used. A closer look at the figure reveals small but interesting discrepancies. It is clear that the measured mobilities (circles for $W_{sp}=0$ nm and squares for $W_{sp}=4.5$ nm) are a little higher than the calculated ones. Since the slight adjustment in the choice of W_{sp} resolves the discrepancies, they are most likely to originate from the surface segregations of Si during the MBE growth, as suggested by Heiblum, Mendez, and Stern[34] and the authors' group.[35] Although the Si segregation process depends on the growth conditions,[35] it gives rise to "extra setback" of the ionized impurities. In the present growth condition, the actual spacer is expected to get thicker than the designed value by about 2 to 3 nm, in good agreement with our result of secondary ion mass spectroscopy (SIMS) measurement.[35] Although the slopes of $\log\mu$-$\log N_s$ characteristics are rather in good agreement with the theory with the exponent $\gamma \sim 1.1$ for $W_{sp}=0$ nm and 1.3 for $W_{sp}=4.5$ nm, we note that the measured data for $W_{sp}=0$ deviate from the theoretical results when $N_s > 5\times10^{11}$ cm^{-2}. This may be attributed to the onset of the intersubband scattering, which is neglected in the calculation. We note also that the exponent γ for $W_{sp}=18.0$ nm is 1.7 and greater than that predicted theoretically ($\gamma \sim 1.5$). The origin of such a discrepancy is not clear at present but is possibly related with the inhomogeneity in the channel, which might result in the extra reduction of μ in the low-N_s region.

Next, we discuss the effects of the substrate bias [or backgating (BG)] on low-temperature mobilities. When the back-gate voltage V_{BG} is applied, it is expected to affect the shape of the wave function and, therefore, μ. To study such effects systematically, we studied μ as a function of both the front-gate (FG) and the back-gate (BG) electric field in a single heterojunction FET structure. In Fig. 8, μ is plotted as a function of N_s, which was varied by the FG electric field, with BG voltage V_{BG} as a parameter. Here, V_{BG} is indicated in parentheses so that, for example, $\mu(-200\text{ V})$ denotes the mobility at $V_{\text{BG}}=-200$ V. It is noted that the deformation of the wave function towards ($V_{\text{BG}}=-200$ V) or away from ($V_{\text{BG}}=+120$ V) the heterointerface leads to the substantial modulation of μ; $\mu(+120\text{ V})$ and $\mu(-200\text{ V})$ differ by as much as 56% at $N_s=2\times10^{11}$ cm^{-2} even when N_s is kept constant.[36] It is also noted that electron confinement enhances the slopes γ of the μ-N_s characteristics. γ increases from 1.25 to 1.47, when V_{BG} is changed from $+120$ to -200 V, which corresponds to the change in N_{depl} from 0 to 1.76×10^{11} cm^{-2}. These data in Fig. 8 are in excellent agreement with the results of theoretical calculations, which are plotted by solid, dashed, and dotted lines. Hence, the observed substrate-bias dependence of μ is well ascribed to the deformation of the electron wave functions, which influences the electron interaction with the scattering potential of the ionized donors.

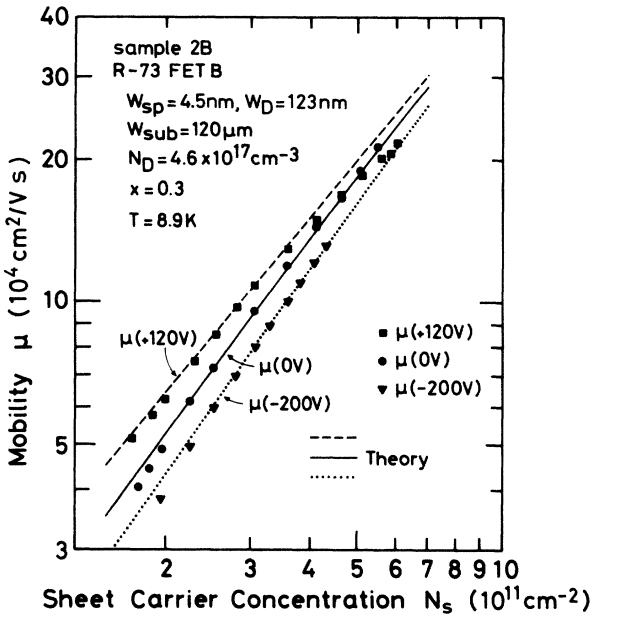

FIG. 8. The electron mobility as a function of electron concentration N_s under different back-bias conditions. Squares for back-gate voltage $V_{\text{BG}}=+120$ V, circles for $V_{\text{BG}}=0$ V, and triangles for $V_{\text{BG}}=-200$ V. N_s was varied by the front-gate voltage.

V. TEMPERATURE DEPENDENCE OF THE MOBILITY

In this section, we study the temperature dependence of the electron mobility mainly below 125 K, where the effect of parallel conduction of the low-mobility electrons in the $Al_xGa_{1-x}As$ is negligibly small.

It is generally accepted that the temperature-dependent part of the electron mobility is mainly dominated by phonon scatterings, since the ionized-impurity scattering process in the highly-degenerate electron system is independent of temperatures. In fact, the mobility limited by polar-optical phonon scattering μ_{PO} and that limited by acoustic-phonon scattering μ_{AC} are theoretically predicted as[10,12,15]

$$\mu_{\text{PO}} \propto T^{-\beta};\ \beta > 2,\ T < 300\text{ K}, \tag{28}$$

$$\mu_{\text{AC}} \propto T^{-1}, \tag{29}$$

phonon scatterings giving rise to a large and negative temperature coefficient in the electron mobility. In Fig. 9(a), inverse mobilities μ^{-1} are plotted as functions of temperature for four different high-mobility samples whose μ is higher than 2×10^5 cm^2/V s at low temperatures.[19] It is clearly seen that μ^{-1} increases linearly with T and can be expressed as $(\mu_0+\alpha T)$ when $T<35$ K. This suggests the dominance of the acoustic-phonon scattering in the temperature-dependent part of μ, as noted by Mendez, Price, and Heiblum.[18] The temperature coefficient α is determined and plotted as a function of N_s by triangles in Fig. 9(b). The data reported by Mendez, Price, and Heiblum[18] are also plotted by circles for comparison. Despite a large variety in structural parameters of samples, the data points of α fall on a single curve and are almost uniquely determined as a function of N_s, as long as the strength of the ionized-impurity scattering is small. This fact suggests the universal nature of phonon scatterings. The determined values of α are somewhat smaller than those calculated with $D=13.5$ eV. This is probably ascribed to the contribution of ionized-impurity scattering, which gives a positive temperature dependence to μ. This will be discussed in the following paragraph. When $T>35$ K, μ^{-1} increases superlinearly with T due to the increasing contribution of the polar-optical phonon scattering in the scattering process.

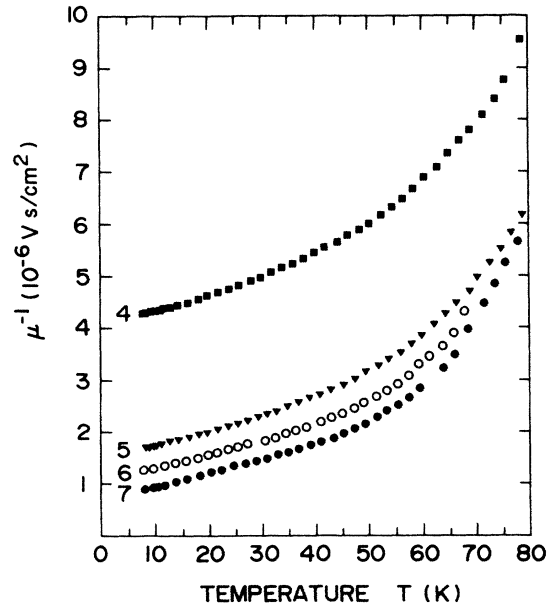

(a)

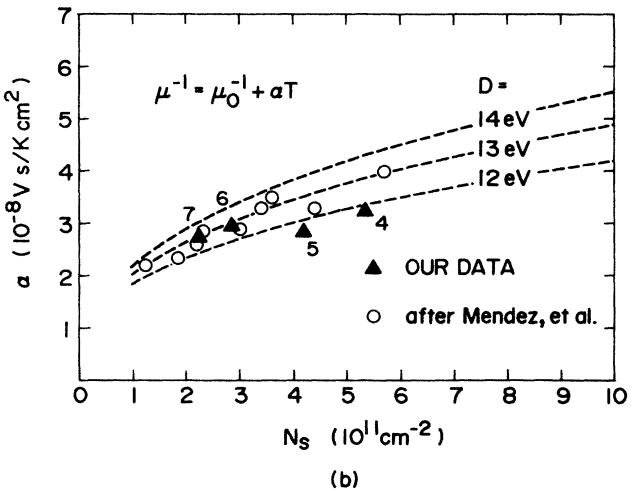

(b)

FIG. 9. (a) Temperature dependences of inverse mobilities μ^{-1} in high-mobility samples ($\mu>2\times10^5$ cm^2/V s) with different electron concentrations. The mobilities and the electron concentrations are controlled only by varying the thickness of spacers, and other structural parameters are identical among these samples (4: R-248-5TA, 5: R-249-5TA, 6: R-250-5TA, 7: R-251-5TA). (b) Temperature coefficient α is plotted by triangles as a function of electron concentration. The results reported by Mendez, Price, and Heiblum (Ref. 18) are also plotted by circles. Dashed lines are theoretical calculations for different values of the deformation-potential constant.

Although the lattice scattering dominates the temperature dependence of μ in high-mobility samples, the situations in low-mobility samples could be substantially different. It is because the ionized-impurity scattering process remains relatively important over the wider temperature range and is expected to play a significant role in the temperature dependence of mobility.[17,19] The mobility limited by the ionized-impurity scattering becomes temperature dependent, when electrons are nondegenerate and their energy varies with temperature. Since the momentum-relaxation time $\tau_I(E)$ due to the ionized-impurity scattering can be expressed approximately as $\tau_I(E)\propto E^\gamma$, it can be shown from preliminary calculation that the mobility $\mu_I(T)$ limited by the ionized-impurity scattering is expressed as

$$\mu_I(T)=\mu_I(0)[1+\pi^2\gamma(\gamma+1)(k_BT/E_F)^2/6]\ ,$$
$$\gamma=1\sim1.5\ , \quad (30)$$

where E_F is the electron Fermi energy, and $\mu_I(0)$ is the mobility limited by the ionized-impurity scattering at $T=0$ K, which depends on E_F and the distribution of scatterers. Equation (30) indicates that the temperature-dependent part of the mobility is positive and a parabolic function of (k_BT/E_F). Hence, this term is strongly dependent on E_F (or carrier concentration N_s) and cannot be neglected unless (k_BT/E_F) is sufficiently small or the $\mu_I(0)$ term is so large that other scattering mechanisms (phonon scattering, in particular) dominate the temperature-dependent part of μ.

In order to evaluate the possible influences of the ionized-impurity scattering on the temperature dependence of mobility, some of the mobility data are extracted from Figs. 3(a)–3(c) and replotted in Figs. 10(a) and 10(b) as functions of temperature for three samples with $W_{sp}=0$ nm (circles), 4.5 nm (squares), and 18.0 nm (triangles). Figure 10(a) shows the mobility data of these samples at $N_s=3\times10^{11}$ cm^{-2}, whereas Fig. 10(b) summarizes the data at $N_s=1.5\times10^{11}$ cm^{-2}. Since N_s is kept constant by the gate-electric field in each set of data, both the spatial extensions of the wave function $f(z)$ and the electron Fermi energy E_F are kept nearly constant. Hence, the contribution of the phonon scatterings within each set

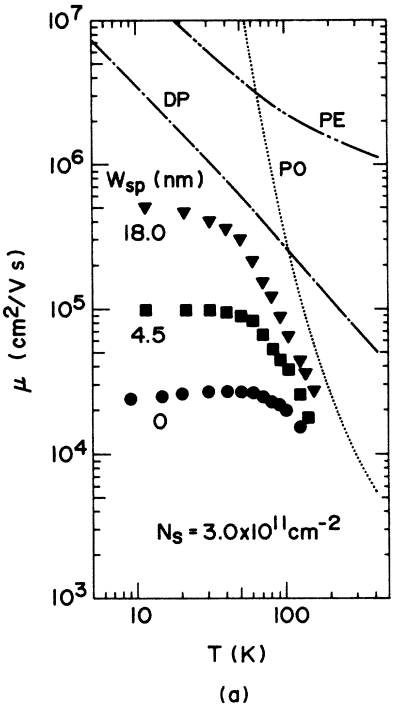

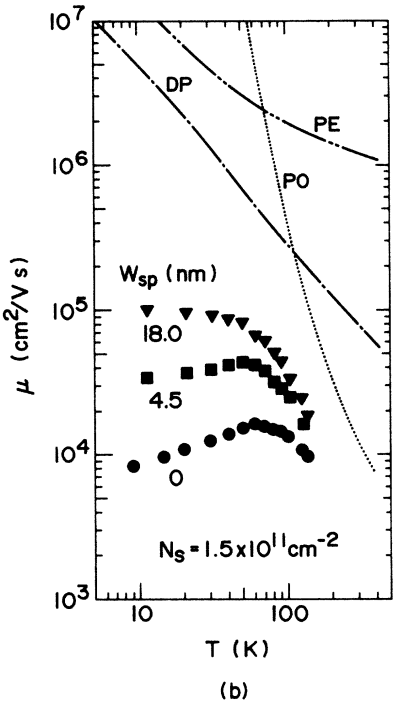

FIG. 10. Temperature dependence of electron mobility μ for three samples with different spacer thickness (triangles for $W_{sp}=18.0$ nm, squares for $W_{sp}=4.5$ nm, and circles for $W_{sp}=0$ nm). In each set of data, N_s is fixed by the gate-electric field. (a) $N_s=3.0\times10^{11}$ cm^{-2}; (b) $N_s=1.5\times10^{11}$ cm^{-2}. Calculated mobilities limited by phonon scatterings are also plotted in the figure by dotted lines. Notations in the figure are the same as in Fig. 4.

of mobility data should be identical, as indicated by theoretical curves in Figs. 10(a) and 10(b). Consequently, the observed differences within each set of data are due exclusively to the differences in the strength of the ionized-impurity scattering among these three samples.

Figure 10(a) indicates that μ of the two samples with thick spacer layers [$W_{sp}=18.0$ nm (triangles) and $W_{sp}=4.5$ nm (squares)] is rather high ($\mu>10^5$ cm^2/V s) and decreases with increasing T when $N_s=3.0\times10^{11}$ cm^{-2} [$E_F=10$ meV; $T_F=120$ K (Fermi temperature)]. This suggests that the temperature dependences of μ in these samples are still dominated by phonon scatterings. The mobility of the sample with no spacer layer (circles), on the other hand, is rather low ($\mu<3\times10^4$ cm^2/V s) and shows a slight increase with T when T is raised up to 40 K, indicating a greater role of the ionized-impurity scattering.

When N_s is reduced down to 1.5×10^{11} cm^{-2} and the kinetic (Fermi) energy E_F of electrons is small ($E_F=5$ meV; $T_F=60$ K), the ionized-impurity scattering is expected to be more effective and give rise to more enhanced positive temperature dependence in mobility. Indeed, Fig. 10(b) clearly shows such a tendency, where a substantial rise of μ is seen at low temperatures ($T<50$ K) not only in the sample with $W_{sp}=0$ nm (circles), but also in the sample with 4.5-nm spacer (squares). This tendency is qualitatively in accordance with what Eq. (30) predicts for the ionized-impurity scattering of nondegenerate electrons. Such a dependence, however, is absent in the sample with $W_{sp}=18.0$ nm, since the ionized-impurity scattering is still efficiently suppressed by the use of a thick spacer layer and overridden by the phonon contribution.

As suggested in Figs. 10(a) and 10(b), the temperature dependence of mobilities depends strongly on the electron concentration N_s (or electron Fermi energy E_F). It is because the reduction of N_s (or E_F) in a single sample leads not only to the enhancement of the $(k_BT/E_F)^2$ term, but also to the reduction of the $\mu_I(0)$ term in Eq. (30), which enhances the role of the ionized-impurity scattering with respect to other scattering mechanisms. To make a systematic study of such N_s dependence of μ, μ in the sample with no spacer layer [sample 1A] is plotted in Fig. 11 as a function of T with N_s as a parameter. It is clearly seen that the temperature dependence of μ for T between 10 and 50 K is negative when $N_s>5\times10^{11}$ cm^{-2} ($E_F>16$ meV), but it becomes increasingly positive as N_s is reduced below 3×10^{11} cm^{-2} ($E_F<10$ meV). This indicates that the temperature dependence of μ is still dominated by the phonon scatterings at the high N_s region, but controlled by the ionized-impurity scattering in the case of low N_s. It should be emphasized that most of the previous experiments have overlooked the presence of such positive temperature dependences, because the simultaneous achievement of low electron concentrations and high impurity concentrations (or thin spacer layers) is difficult unless N_s is controlled by the gate voltage as done in this work. The tendencies shown in Fig. 11 are in accordance with our theoretical predictions and demonstrate the importance of the temperature-dependent part of the ionized-impurity scattering in the case when the electron

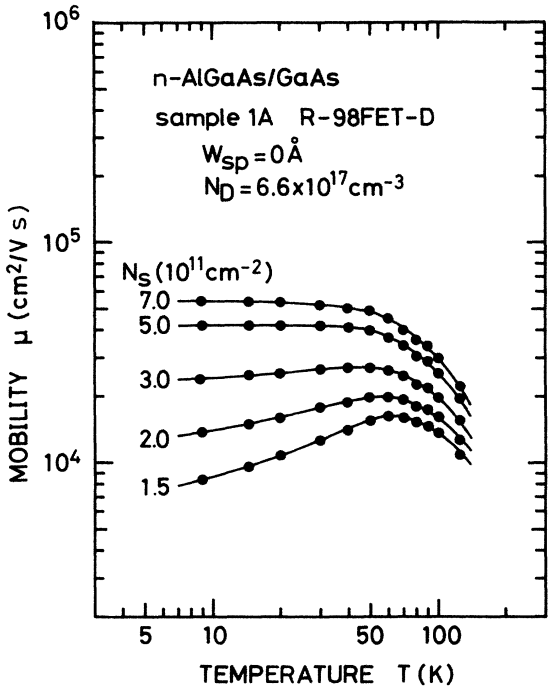

FIG. 11. Temperature dependence of electron mobility μ for the sample with no spacer. N_s is a parameter.

concentration is reduced in the samples with thin spacers. Although this situation appears to be rather unusual, it is a situation commonly encountered in practical heterojunction FET's whenever they switch from on-state to off-state, or vice versa, in electronic circuits.

VI. IN SUMMARY

The mobility μ of the two-dimensional electron gas is systematically studied as a function of electron concentration N_s as well as temperature T with the thickness of the spacer W_{sp} as a parameter. N_s is varied by using the gate electric field in FET configurations in order to eliminate the ambiguities of the impurity distributions and realize all the possible situations encountered in FET operations. Consequently, it is found that:

(i) μ increases with increasing N_s in the entire temperature range studied here (10 K $< T <$ 300 K), as long as the effect of parallel conduction of the low-mobility electrons in the $Al_xGa_{1-x}As$ is negligibly small.

(ii) The slopes of the μ-N_s characteristics become steeper with decreasing T when $T <$ 125 K, suggesting that the ionized-impurity scattering becomes more dominant at lower temperatures.

(iii) The mobility μ and its dependence on N_s measured at low temperatures are found to be well explained by the existing theory of the ionized-impurity scattering.

(iv) When $T <$ 40 K, the temperature dependence of μ is negative in the samples with larger W_{sp} and/or higher N_s and is dominated by the acoustic-phonon scattering. When N_s is reduced in samples with smaller W_{sp}, however, the ionized-impurity scattering dominates the temperature dependence of μ, resulting in a substantial increase of μ with increasing T.

(v) Some of the unresolved problems are pointed out, including the substantial rise of μ with the increase of N_s at intermediate and high temperatures, which appear to call for further developments in the theory of phonon scatterings.

ACKNOWLEDGMENTS

We wish to express our sincere thanks to Professor T. Ando for many stimulating discussions related to his calculations. We thank Professor S. Kawaji and Dr. J. Yoshino for useful discussions, and Dr. J. Wakabayashi for low-temperature measurement. Professor J. Hamasaki, T. Matsusue, and Y. Sekiguchi are also acknowledged for their constant encouragement. One of the authors (K.H.) thanks the Japan Society for the Promotion of Science for partial financial support. This work is mostly supported by a Grant-in-Aid from the Ministry of Education, Science, and Culture, Japan.

[1]H. L. Stormer, R. Dingle, A. C. Gossard, W. Wiegmann, and M. D. Sturge, Solid State Commun. **29**, 705 (1979).
[2]S. Hiyamizu, J. Saito, K. Nanbu, and T. Ishikawa, Jpn. J. Appl. Phys. **22**, L609 (1983).
[3]J. C. M. Hwang, A. Kastalsky, H. L. Stormer, and V. G. Keramidas, Appl. Phys. Lett. **44**, 802 (1984).
[4]N. Sano, H. Kato, and S. Chika, Solid State Commun. **49**, 123 (1984).
[5]T. Ando, A. B. Fowler, and F. Stern, Rev. Mod. Phys. **54**, 499 (1982).
[6]T. Ando, J. Phys. Soc. Jpn. **51**, 3900 (1982).
[7]P. J Price, Ann. Phys. (N.Y.) **133**, 217 (1981).
[8]P. J Price, Surf. Sci. **113**, 199 (1982).
[9]P. J Price, Surf. Sci. **143**, 145 (1984).
[10]K. Lee, M. S. Shur, T. J. Drummond, and H. Morkoc, J. Appl. Phys. **54**, 6432 (1983).
[11]F. Stern, Appl. Phys. Lett. **43**, 974 (1983).
[12]W. Walukiewicz, H. E. Ruda, J. Lagowski, and H. C. Gatos, Phys. Rev. B **30**, 4571 (1984).
[13]P. K. Basu and B. R. Nag, Phys. Rev. B **22**, 4849 (1980).
[14]B. K. Ridley, J. Phys. C **15**, 5899 (1982).
[15]B. Vinter, Appl. Phys. Lett. **45**, 581 (1984).
[16]P. J. Price, Phys. Rev. B **30**, 2234 (1984).
[17]M. A. Paalanen, D. C. Tsui, A. C. Gossard, and J. C. M. Hwang, Phys. Rev. B **29**, 6003 (1984).
[18]E. E. Mendez, P. J. Price, and M. Heiblum, Appl. Phys. Lett. **45**, 294 (1984).
[19]B. J. F. Lin, D. C. Tsui, M. A. Paalanen, and A. C. Gossard, Appl. Phys. Lett. **45**, 695 (1984).
[20]H. L. Stormer, A. C. Gossard, W. Wiegmann, and K. Baldwin, Appl. Phys. Lett. **39**, 912 (1981).
[21]G. Weimann and W. Schlapp, Appl. Phys. Lett. **46**, 411

(1985).
[22]F. Stern, Phys. Rev. B **5**, 4891 (1972).
[23]D. L. Rode, in *Semiconductors and Semimetals,* edited by R. K. Willardson and A. C. Beer (Academic, New York, 1975), Vol. 10.
[24]F. Stern, Phys. Rev. Lett. **44**, 1469 (1980).
[25]P. F. Maldague, Surf. Sci. **73**, 296 (1978).
[26]K. Hirakawa, H. Sakaki, and J. Yoshino, Appl. Phys. Lett. **45**, 253 (1984).
[27]B. Vinter, Appl. Phys. Lett. **44**, 307 (1984).
[28]K. Lee, M. S. Shur, T. J. Drummond, and H. Morkoc, IEEE Trans. Electron Devices, **ED-31**, 29 (1984).
[29]A. J. Valois, G. Y. Robinson, K. Lee, and M. S. Shur, J. Vac. Sci. Technol. **B1**, 190 (1983).
[30]See, for example, M. O. Watanabe, K. Morizuka, M. Mashita, Y. Ashizawa, and Y. Zohta, Jpn. J. Appl. Phys. **23**, L103 (1984).
[31]F. F. Fang and A. B. Fowler, Phys. Rev. **169**, 619 (1968).
[32]H. Ezawa, S. Kawaji, T. Kuroda, and K. Nakamura, Surf. Sci. **24**, 659 (1971).
[33]Y. Sekiguchi, H. Sakaki, T. Tanoue, T. Hotta, and H. Ohno, in *Collected Papers of the Second International Symposium on Molecular Beam Epitaxy and Related Clean Surface Techniques, Tokyo,* edited by R. Ueda (Applied Physics Society of Japan, Tokyo, 1982), p. 139.
[34]M. Heiblum, E. E. Mendez, and F. Stern, Appl. Phys. Lett. **44**, 1064 (1984).
[35]K. Inoue, H. Sakaki, J. Yoshino, and Y. Yoshioka, Appl. Phys. Lett. **46**, 973 (1985).
[36]K. Hirakawa, H. Sakaki, and J. Yoshino, Phys. Rev. Lett. **54**, 1279 (1985).